DOI: https://doi.org/10.37434/tpwj2024.02.01

MICROHARDNESS AND CORROSION PROPERTIES OF FRICTION STIR WELDED PHOSPHOR BRONZE

S. Gopi[1], **D.G. Mohan**[2]

[1]Department of Production Engineering, Government College of Technology
Coimbatore, Tamilnadu, India, 641013
[2]School of Engineering Faculty of Technology, University of Sunderland
England, United Kingdom - SR6 0DD

ABSTRACT

This study investigates the microhardness and corrosion properties of friction stir welded (FSW) joints in phosphor bronze ($CuSn_4$), a vital non-ferrous alloy in engineering applications. The research delves into the FSW process, employing varying welding parameters to create joints that exhibit distinct microstructural characteristics. Microhardness distribution across the FSW joints is assessed and correlated with the base material's properties. Corrosion behaviour is rigorously examined through weight loss tests, revealing insights into the susceptibility of FSW joints to various corrosive environments. The study identifies the influence of FSW parameters on microhardness and corrosion performance, thus contributing to understanding the alloy's behaviour under this welding technique. This research shows that the welding speed of 0.25 mm/s, tool rotational speed of 1100 rpm, plunger depth of 0.2 mm, and a hexagonal tool profile produce the better joint with the highest microhardness of 139 *HV* and rate of corrosion of 0.420831 %.

KEYWORDS: friction stir welding, phosphor bronze, corrosion, microhardness, joining

INTRODUCTION

Phosphor bronze, an intricately formulated bronze alloy, has garnered widespread recognition due to its exceptional amalgamation of properties. Its elevated strength and hardness render it a fitting choice for structural components that endure substantial loads. This alloy's intrinsic resistance to corrosion causes it an optimal material for marine apparatus and plumbing systems, imparting longevity and reliability to such critical installations [1]. Phosphor Bronze's inherent resistance to wear qualifies it for pivotal roles in bearings and gears, while its commendable machinability facilitates intricate shaping with ease. Notably, this alloy boasts superior thermal and electrical conductivity, a crucial attribute that finds practical utility in heat exchangers and electrical connectors. The myriad characteristics of Phosphor Bronze collectively position it as the preferred material across industries that demand a harmonious blend of strength, corrosion resistance, wear resilience, machinability, and aesthetic allure [2].

Friction Stir Welding (FSW), an innovative solid-state welding technique, has emerged as an exceedingly promising approach for joining Phosphor Bronze, presenting distinct advantages over conventional fusion welding methodologies. Operating beneath the melting threshold of the materials involved, FSW ensures the retention of Phosphor Bronze's intrinsic properties [3, 4]. This autogenous and continuous process harnesses a non-consumable spinning tool distinguished by its superior hardness relative to the Phosphor Bronze. It generates frictional heat and mechanical agitation to effectuate seamless material fusion [5, 6]. Applying FSW to Phosphor Bronze welding yields a spectrum of noteworthy benefits. By circumventing prevalent challenges inherent to fusion welding, such as oxidation and porosity, FSW orchestrates material fusion in the solid state, curtailing Phosphor Bronze's interaction with oxygen. This prudent measure averts the formation of deleterious oxide layers and porosity, resulting in immaculate welds characterised by heightened structural integrity and diminished imperfections.

Moreover, FSW affords meticulous management of heat input throughout the welding process, curbing distortion and preserving Phosphor Bronze's mechanical attributes [7]. The absence of filler metals simplifies the welding procedure, concurrently curtailing material expenses. Additionally, the mechanical agitation intrinsic to FSW promotes material homogenisation, fortifying joint strength and integrity [8]. As applied to Phosphor Bronze welding, FSW's salient virtues engender it as an enticing alternative to fusion-based welding methodologies across various applications. The solid-state predilection of FSW underscores the safeguarding of material properties, engendering superior control over the heat-affected zone (HAZ) while mitigating thermal distortion.

Besides, the obviation of fusion-induced flaws, exemplified by solidification cracks, augments overall weld joint robustness and endurance [9]. These attributes bear heightened significance when considering Phos-

Table 1. Chemical compositions of $CuSn_4$

Cu, %	Sn, %	Zn, %	Fe, %	P, %	Ni, %	Si, %	Mn, %
96.32	3.45	0.1	0.012	0.740	0.012	0.063	0.0072

phor Bronze, a material hailed for its distinct mechanical and corrosion-resistant traits. The amelioration of typical concerns associated with fusion welding, encompassing oxidation and porosity, culminates in high-calibre welds distinguished by augmented structural integrity and elevated corrosion resistance [10]. The deployment of FSW in welding Phosphor Bronze has the potential to significantly enhance performance and dependability across industries reliant on welded components.

Nevertheless, a conspicuous research void remains in FSW applied to Phosphor Bronze joining. In addressing this lacuna, this research explores the intricacies of joining phosphor bronze through FSW techniques. This study's primary focus lies in the exhaustive analysis of microhardness and corrosion properties — a comprehensive exploration offering invaluable insights into the efficacy and aptness of these welding methodologies vis-à-vis the unique attributes of phosphor bronze. Through this pursuit, a definitive stride is taken towards expanding the frontiers of knowledge surrounding the application of FSW to enrich phosphor bronze's role in many industrial applications.

EXPERIMENTAL METHODOLOGY

This research work was carried out using a phosphor bronze (CuSn4). To facilitate the examination, plates having dimensions of 4mm in thickness, 100 mm in length, and 50mm in width were chosen for FSW. The resultant welds assumed the form of butt joints, meticulously crafted along the axis of lamination under standard atmospheric conditions [11]. The chemical compositions of the specimens have been given in Table 1.

The FSW procedures were executed utilising a vertical milling machine, thereby furnishing a stable and meticulously controlled platform to facilitate the welding process. A non-consumable carbide tool was selected for these operations, with a pin length of 3.6 mm and a pin diameter of 2.6 mm, encompassing three distinct pin profiles — square, pentagon, and hexagon and the shoulder, with a diameter of 25 mm and a flat face, was employed [12]. This rigorous selection process aims to ensure optimal efficacy within this study. A singular-pass welding methodology was used to uphold uniformity and mitigate potential disparities, thereby generating joints of consistent quality and fostering dependable scrutiny of ensuing weld attributes. The definitive process parameters were established post iterative trials and a thorough review of pertinent literature. Consequently, the finalised FSW parameters encompassed a welding speed of 0.25 mm/s, a tool rotational speed of 1100 rpm, a plunge depth of 0.2 mm, and the utilisation of three distinct tool profiles — square, pentagon, and hexagon, each bearing a flat shoulder. Figure 1 shows the FSW process on phosphor bronze plates.

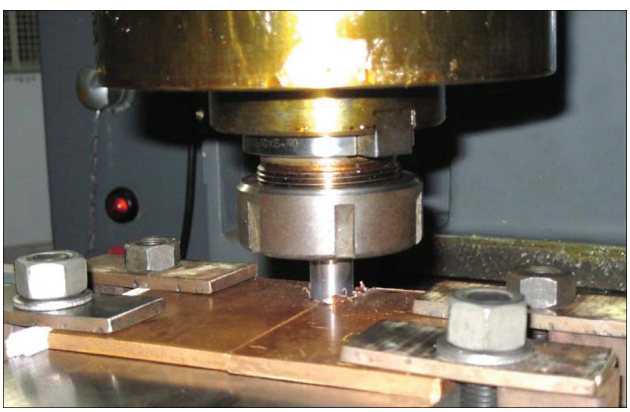

Figure 1. FSW setup with phosphor bronze plates

The FSW joints were subjected to meticulous sectioning along the transverse direction to enable an exhaustive assessment. This controlled sectioning procedure effectively segregated the weld bead and the HAZ from the parent alloy, which is essential for nuanced evaluation. In preparation for corrosion testing, the specimens were meticulously embedded within epoxy resin, thereby confining exposure exclusively to the welded surface, a prerequisite for precise corrosion behaviour evaluation. The specimens underwent successive polishing with emery papers, culminating at a grit size of 1000, thereby guaranteeing the elimination of any extraneous surface impurities or irregularities. Subsequently, a specialised degreaser was employed, achieving a smooth, pristine surface conducive to subsequent characterisation and evaluation. Adhering to ASTM E384 standards, microhardness assessments were systematically conducted for all weldments [13].

Further advancing the analytical process, a weight loss corrosion test was executed in adherence to ASTM G31 standards. The subsequent immersion of the joints' weld zones within 3.5 wt.% sodium chloride solution transpired in individual 500 ml beakers maintained at ambient temperature [14]. This strategic approach provides accurate insights into the corrosion behaviour of the joint.

RESULTS AND DISCUSSION

The FSW operations were performed on a vertical milling machine, providing a stable and controlled platform for the welding process. A non-consumable carbide tool with a pin length of 3.6 mm, a pin diameter of 2.6 mm with three different pin profiles (square, pentagon and hexagon) and a shoulder diameter of 25 mm with a flat face is adopted for this work [15]. Specimen S1

used a square pin profile, S2 used a hexagon pin profile, and S3 used pentagon pin profiles for the FSW process. A single-pass welding technique was employed to fabricate the joints, ensuring uniformity and enabling reliable analysis of the resulting weld characteristics. The process parameters are finalised after conducting trial runs and a literature review. The process parameters selected for FSW are weld speed of 0.25 mm/s, tool rotational speed of 1100 rpm, plunge depth of 0.2 mm and three different tool profiles, square, pentagon and hexagon with flat shoulder.

The FSW joints were carefully sectioned in the transverse direction to obtain representative specimens for analysis. The sectioning process involved cutting along the welding direction, effectively separating the weld bead and the HAZ from the parent alloy. In order to conduct corrosion testing, the specimens were embedded in epoxy resin, ensuring that only the welded surface was exposed to the salt solution, thereby facilitating an accurate assessment of the corrosion behaviour [16]. The specimens were initially cleaned using emery papers up to a grit size of 1000, ensuring the removal of any surface impurities or irregularities. Finally, a degreaser was applied to achieve a smooth and pristine surface, ready for subsequent characterisation and evaluation. Microhardness was conducted for all the weldments made with the optimised input variables following ASTM E384 standards. The weight loss corrosion test was conducted per ASTM G31 standards. After cleaning, the metal samples are blow-dried and weighed. After initial weighing of all the FSW samples, they were suspended, and the weld zones were immersed into 500 ml beakers containing 3.5 wt.% sodium chloride solution separately at room temperature.

In the current Fabricated Friction Stir Welding (FFSW) joints investigation, dissecting and addressing two distinct phenomena inherently yield disparate outcomes is imperative. The first of these phenomena centres around the temperatures to which the materials are subjected during welding. Although these temperatures remain below their respective melting points, the consequences on mechanical properties are undeniable. This influence extends across critical regions, including the nugget, Thermal-Mechanically Affected Zone (TMAZ), and HAZ.

Conversely, the second phenomenon hinges upon the substantial shear stresses engendered by the dynamic motion of the welding tool. This mechanical agitation induces the formation of an exceedingly refined microstructure, a phenomenon prominently manifested within the nugget zone and predominantly evident within the flow arm zone. The outcome is a partial restoration of mechanical properties, marking a discernible pattern of variation as one traverses from the central axis of the weld bead, traverses the TMAZ, and transitions into the HAZ. An intriguing aspect comes to the fore when investigating FSW joints in phosphor bronze alloys akin to those scrutinised herein, as exemplified by the S2 sample [17]. Here, the relatively lower temperatures endured during the welding process can incite a form of ageing that, in turn, leads to a modest yet discernible enhancement in mechanical characteristics.

Ascertaining corrosion properties is integral to this inquiry, where the mass of specimens before and after corrosion, coupled with corresponding percentage weight losses, is provided in Table 2. This calculation of corrosion-induced weight loss aligns with the established rate of corrosion formulas. The pre-corrosion and post-corrosion masses of the welds are judiciously measured, and the resultant weight loss is presented as a percentage relative to the parent weld's mass. The data in Table 2 shows the corrosion behaviour exhibited by the specimens subjected to the weight loss test. A notable trend emerges, notably the substantially lower weight loss attributed to corrosion in FSW samples such as S2, as discerned through meticulous analysis over a 14-day duration [18].

Of particular significance, the representative FSW weld, Specimen S2, exhibits an admirably lesser weight loss of 0.420831 %, a distinctive marker of high corrosion resistance. Corrosion behaviour is governed by an array of factors encompassing temperature, corrosive agent concentration, diffusion rates, and the presence of oxidising agents [19]. These determinants collectively dictate a material's susceptibility to corrosion processes. Beyond these well-established influences, the corrosion resistance of metals is linked to microstructural attributes.

Precisely, the grain size and the presence of precipitated particles wield significant sway over material corrosion properties. A finer grain structure, often achievable through the unique thermomechanical conditions inherent to FSW, can potentiate augmented corrosion resistance by reduced grain boundary pres-

Table 2. Mass of the specimens before and after corrosion of weight loss, %

Specimens	Mass before corrosion, g	Mass after corrosion, g	Weight loss due to corrosion, %
S1 (Square pin)	14.489	8.1265	0.439126
S2 (Hexagon pin)	16.888	9.7810	0.420831
S3 (Pentagon pin)	14.566	7.9640	0.453247

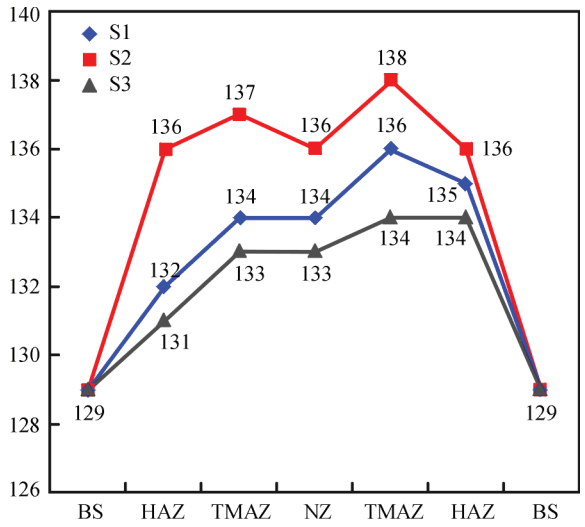

Figure 2. Microhardness of FSW specimen

ence and the concomitant curbing of preferential sites for corrosion initiation [20, 21]. Additionally, the impact of precipitated particles, including second-phase and precipitates stemming from the welding process, cannot be understated. These entities can significantly influence local electrochemical behaviour, subsequently modifying a material's corrosion susceptibility. The amalgamation of grain size refinement and precipitate formation in FSW-welded materials contributes to the heightened corrosion performance observable in Specimen S2.

Conversely, the data elucidated within Table 2 accentuates the remarkable corrosion resistance manifested in the FSW specimens, with Specimen S2 serving as a poignant exemplar in contrast to alternative joints. Although factors such as temperature and chemical environment retain their cardinal roles in corrosion, the salient contribution of microstructural attributes — precisely grain size and precipitate presence — must not be trivialised [22]. This comprehensive comprehension of corrosion behaviour is instrumental in optimising welding processes to elevate material performance and longevity within corrosive settings.

All experimental undertakings involving friction stir were meticulously orchestrated under controlled ambient conditions, maintaining a steady temperature of 30 °C. In the context of the FSW specimens, a notable thermal polarity becomes evident, with the advancing side (AS) registering heightened heat generation relative to the retreating side (RS). This distinctive phenomenon is attributed to the rotational dynamics of the tool, orchestrating the movement of relatively colder material from the AS to the RS. Accordingly, when effecting the fusion of phosphor bronze, strategic placement of the alloy material within the RS is judiciously employed to harness enhanced strength generation at the AS, thereby fostering comprehensive mechanical robustness within the welded interconnections [23]. A graphical representation of average microhardness attributes within butt joints constructed from phosphor bronze through FSW is elegantly presented in Figure 2.

Prominently, Sample S2 emerges as a beacon of elevated joint tensile strength. This pinnacle achievement is underscored by the implementation of specific parameters, notably a tool rotation rate of 1100 rpm, a welding speed of 0.25 mm/s, and a plunge depth of 0.2 mm. Specimen S2 attains the average microhardness of 137 *HV*. It is discernible that the retreating side distinctly boasts heightened microhardness within the TMAZ region, a consequence of the complex interplay between thermomechanical dynamics and resultant grain modification within this domain [24].

CONCLUSION

This study comprehensively explores microhardness and corrosion attributes in FSW joints using phosphor bronze ($CuSn_4$). The study effectively elucidates FSW parameter impact on microhardness and corrosion, enhancing understanding of alloy behaviour in this welding context.

Notably, optimal parameters of welding speed (0.25 mm/s), tool rotational speed (1100 rpm), plunge depth (0.2 mm), and hexagonal tool profile yield exceptional outcomes. These parameters engender superior microhardness (139 *HV*) and minimal corrosion rate (0.420831 %), showcasing their instrumental role in attaining favourable joint attributes.

This study underscores FSW's profound influence on microhardness and corrosion in phosphor bronze joints while highlighting the strategic orchestration of welding parameters. This contribution augments the evolving understanding of FSW's potential, refining material attributes for targeted performance prerequisites.

REFERENCES

1. Hu, D., Chen, M., Wang, L. et. al. (2016) Dynamic tensile behaviour and deformational mechanism of C5191 phosphor bronze under high strain rates deformation. *Materials Sci. and Eng.: A*, **649**, 68–73. DOI: https://doi.org/10.1016/j.msea.2015.09.075
2. Khan, N.Z., Siddiquee, A.N., Khan, Z.A. et. al. (2021) Improvement in joint efficiency with high productivity and narrow weld formation in friction stir welding. Proceedings of the Institution of Mechanical Engineers, Pt E. *J. of Process Mechanical Eng.*, 095440892110424. DOI: https://doi.org/10.1177/09544089211042480
3. Zoeram, A.S., Anijdan, S.H.M., Jafarian, H.R. et. al. (2017) Welding parameters analysis and microstructural evolution of dissimilar joints in al/bronze processed by friction stir welding and their effect on engineering tensile behavior. *Materials Sci. and Eng.: A*, **687**, 288–297. DOI: https://doi.org/10.1016/j.msea.2017.01.071

4. Mohan, D.G., Wu, C. (2021) A review on friction stir welding of steels. *Chinese J. of Mechanical Eng*., 34(**1**). DOI: https://doi.org/10.1186/s10033-021-00655-3
5. Rabiezadeh, A., Salafzon, A., Mostafavi, N. (2023) Dissimilar welding of AA5083/AA7039 by self-reacting friction stir welding. *J. of Adhesion Sci. and Technology*, 1–22. DOI: https://doi.org/10.1080/01694243.2023.2219367
6. Sasikumar, A., Gopi, S., Mohan, D.G. (2022) Prediction of filler added friction stir welding parameters for improving corrosion resistance of dissimilar aluminium alloys 5052 and 6082 joints. *Advances in Materials Sci.*, 22(**3**), 79–95. DOI: https://doi.org/10.2478/adms-2022-0014
7. Yin, K., Cao, L., Wang, N. (2019) Mechanical properties and residual stresses of 5083 to AM60B dissimilar friction stir welding with different process parameters. *J. of Adhesion Sci. and Technology*, 33(**23**), 2615–2629. DOI: https://doi.org/10.1080/01694243.2019.1653593
8. Çam, G. (2011) Friction stir welded structural materials: Beyond al-alloys. *Inter. Materials Reviews*, 56(**1**), 1–48. DOI: https://doi.org/10.1179/095066010x12777205875750.
9. Shokri, V., Sadeghi, A., Sadeghi, M. H. (2017) Effect of friction stir welding parameters on microstructure and mechanical properties of DSS–cu joints. *Materials Sci. and Eng.: A*, **693**, 111–120. DOI: https://doi.org/10.1016/j.msea.2017.03.054
10. Liu, H. J., Shen, J. J., Zhou, L., et. al. (2011) Microstructural characterisation and mechanical properties of friction stir welded joints of aluminium alloy to copper. *Sci. and Technology of Welding and Joining*, 16(**1**), 92–98. DOI: https://doi.org/10.1179/1362171810y.0000000007
11. Vinith, B., Dharshan, S. A., Aravind, S. et. al. (2023) Friction stir welding evolution, hybrid technologies and shoulder shape. *Inter. J. on Interactive Design and Manufacturing*, 17(**4**), 1443–1458. DOI: https://doi.org/10.1007/s12008-023-01208-9
12. Mohan, D. G., Tomków, J., Gopi, S. (2021). Induction assisted hybrid friction stir welding of dissimilar materials AA5052 aluminium alloy and X12Cr13 stainless steel. *Advances in Materials Sci*., 21(**3**), 17–30. DOI: https://doi.org/10.2478/adms-2021-0015
13. Wang, Q., Zhou, X., Wang, B. et. al. (2023) Accelerated role of exogenous riboflavin in Selective desulfovibrio desulfuricans corrosion of pipeline welded joints. *Bioelectrochemistry*, **153**, 108469. DOI: https://doi.org/10.1016/j.bioelechem.2023.108469
14. Liu, P., Li, Y., Geng, H. et. al. (2007) Microstructure characteristics in TIG welded joint of Mg/Al dissimilar materials. *Materials Letters*, 61(**6**), 1288–1291. DOI: https://doi.org/10.1016/j.matlet.2006.07.010
15. Gopi, S., Mohan, D.G. (2021) Evaluating the welding pulses of various tool profiles in single-pass friction stir welding of 6082-T6 aluminium alloy. *J. of Welding and Joining*, 39(**3**), 284–294. DOI: https://doi.org/10.5781/jwj.2021.39.3.7
16. Yelamasetti, Balrm, Adithya, G.S., Ramadevi, R.S. et. al. (2023) Metallurgical, mechanical and corrosion behaviour of pulsed and constant current TIG dissimilar welds of Aisi 430 and Inconel 718. *J. of Materials Research and Technology*, **24**, 6652–6664. DOI: https://doi.org/10.1016/j.jmrt.2023.04.231
17. Tamadon, A., Pons, D.J., Clucas, D. (2020) Analogue modelling of flow patterns in bobbin friction stir welding by the dark-field/bright-field illumination method. *Advances in Materials Sci.*, 20(**1**), 56–70. DOI: https://doi.org/10.2478/adms-2020-0003
18. Yelamasetti, Balram, Vardhan, T.V., Ramana, G.V. (2020) Study of metallurgical changes and mechanical properties of dissimilar weldments developed by interpulse current TIG welding technique. Proceedings of the Institution of Mechanical Engineers, Pt C: *J. of Mechanical Eng. Sci*., 235(**16**), 2985–2997. DOI: https://doi.org/10.1177/0954406220960780
19. Xuan, Y., Yang, J., Liu, H. et. al. (2020) Microstructure and mechanical properties of Invar36 alloy joints using keyhole TIG welding. *Sci. and Technology of Welding and Joining*, 25(**8**), 712–718. DOI: https://doi.org/10.1080/13621718.2020.1830545
20. Dhondt, M., Aubert, I., Saintier, N. et. al. (2011) Intergranular stress corrosion cracking of friction stir welded nugget on a 2050-T8 aluminum alloy. *Advances in Materials Sci.*, 11(**3**). DOI: https://doi.org/10.2478/v10077-011-0016-6
21. Kusano, K., Watanabe, H. (2002) Recent trends in development of high-efficiency TIG welding; high-deposition TIG welding and ultranarrow-gap TIG welding. *Welding Inter.*, 16(**12**), 986–991. DOI: https://doi.org/10.1080/09507110209549651
22. Dudzik, K., Jurczak, W. (2015) Influence of friction stir welding on corrosion properties of AW-7020M alloy in sea water. *Advances in Materials Sci.*, 15(**1**), 7–13. DOI: https://doi.org/10.1515/adms-2015-0002
23. Zhou, D., Xia, Y., Gao, Z. et. al. (2023) Effect of loading conditions on corrosion fatigue process of FSW AA6061-T6 joint in 3.5 % NaCl studied by electrochemical noise. *J. of Materials Research and Technology*, **24**, 9808–9823. DOI: https://doi.org/10.1016/j.jmrt.2023.05.179
24. Qiu, Y., Yang, X., Xu, J. et. al. (2022) Enhanced mechanical property and corrosion resistance of alloy 5182 fsw joints by SC and ZR alloying. *Materials Characterization*, **194**, 112412. DOI: https://doi.org/10.1016/j.matchar.2022.112412

ORCID
S. Gopi: 0000-0002-4652-4198,
D.G. Mohan: 0000-0001-7966-1853

CONFLICT OF INTEREST
The Authors declare no conflict of interest

CORRESPONDING AUTHOR
D.G. Mohan
School of Engineering Faculty of Technology,
University of Sunderland, England,
United Kingdom - SR6 0DD.
E-mail: dhanesh.mohan@sunderland.ac.uk

SUGGESTED CITATION
S. Gopi, D.G. Mohan (2024)
Microhardness and corrosion properties of friction stir welded phosphor bronze. *The Paton Welding J*., **2**, 3–7.

JOURNAL HOME PAGE
https://patonpublishinghouse.com/eng/journals/tpwj

Received: 23.08.2023
Received in revised form: 26.12.2023
Accepted: 31.01.2024